

Influence of scaling effects on designing for power efficiency of a micropreconcentrator

K. A. Cook

Department of Biomedical Engineering, University of Michigan, Ann Arbor, Michigan 48109

A. M. Sastry^{a)}

Department of Biomedical Engineering and Department of Mechanical Engineering, University of Michigan, Ann Arbor, Michigan 48109

(Received 30 June 2004; accepted 14 February 2005; published 6 April 2005)

Rapid and reliable assessment of volatile and semivolatile organic compounds in the environment using gas chromatography (GC) is often limited by cost of analysis, and time delays between sampling and analysis. Many environmental monitors incorporating GC systems are too large for portability, and lack sufficient sensitivity and/or selectivity to serve as practical environmental monitors. Frequently, a complete system redesign, due to nonlinear power scaling relative to component size, is required to reduce the mass and volume of power supplies, especially for the micro-systems of present interest. Here, we examined four strategies in reducing power demand by the largest consumer of power in a model micro GC, the preconcentrator. Our simulations included alterations in heater pad placement/size, reduction of thermal mass in the device, vacuum sealing, and incorporation of a gas dwell time during preconcentrator heating. Our numerical results were in general agreement with experimental findings in simpler systems, in terms of the benefits of vacuum sealing. The greatest reductions in power demand were achieved with vacuum sealing (51%) and reductions in thermal mass (15%). Future work will address structural and materials issues involved in reduction of thermal mass, and also optimization of power supplies required to meet the multilevel power demands of these complex microelectromechanical systems. © 2005 American Vacuum Society. [DOI: 10.1116/1.1886821]

I. INTRODUCTION

Rapid and reliable assessment of volatile and semivolatile organic compounds in the environment using gas chromatography (GC) is often limited by cost of analysis, and time delays between sampling and analysis. Many environmental monitors incorporating GC systems are too large for portability, and lack sufficient sensitivity and/or selectivity to serve as practical environmental monitors.^{1,2} Onboard power supplies in these systems, whose volume and mass often limit the ultimate device size,³ are an important target for reduction. Frequently, a complete system redesign, due to nonlinear power scaling relative to component size, is required to reduce the mass and volume of power supplies.⁴

Most GC systems are comprised of seven components: carrier gas, flow controller, sample inlet/preconcentrator, one or more columns, controlled temperature zones (ovens), detectors, and data acquisition system. Field-portable designs have been proposed that exploit reductions in volumes of GC systems by replacement of carrier gases (e.g., helium or hydrogen) with environmental air,⁵⁻⁷ other designs have incorporated miniaturized components to improve portability.⁸⁻¹⁰ GC sensing is based on differential migration of bands of molecules injected into the high pressure end of a column, as a concentrated volume (plug) of sample. A table of typical sample volumes for columns is given in Table I.¹¹ Microsen-

sors typically consist of Au-thiolate monolayers encapsulated by metal nanoclusters, with different thin film resistances and sensitivities to reversibly adsorb organic vapors. Thus, the signal from the column is measured as a voltage difference, due to change in resistance of the microsensor upon exposure to the analyte. Signals or peaks correspond to retention time or fractional volume of a component of the sample, and are Gaussian in shape. Excessively high bandwidths prevent accurate analysis of species, and reduction in volume of analyte usually requires that gases be preconcentrated.

Wise, Angell, and Terry, and Jerman were the first group to demonstrate that key GC components, including the column and detector, could be fabricated on silicon, paving the way for development of microgas chromatograph (μ GC) systems.^{12,13} Since then, other workers have similarly constructed μ GC columns,^{10,14,15} heaters,^{9,16} sensors,^{17,18} and thermal conductivity detectors¹⁹ on silicon wafers. Design of a near-real time, fully integrated μ GC remains a challenge, however; elimination of memory effects, shortening of time response, and achievement of high sensitivity, selectivity, reproducibility, and system stability over time are all important design goals in such a device. But perhaps the most important barriers to realization of a μ GC are reduction of power demand by individual components, and implementation of an onboard, low volume and low mass power supply system.

Here, we used simulations to identify likely means of power reduction, in a specific μ GC system, which uses air as both carrier and analyte gas using data provided by Lu and

^{a)}Author to whom correspondence should be addressed; electronic mail: amsastry@umich.edu

TABLE I. Typical sample volumes for various types of GC columns.

Column type	Sample size (liquid)
Regular analytical packed: 0.25 in. outer diameter, 10% liquid	0.2–20.0 μl
High efficiency packed: 0.225 in. outer diameter, 3% liquid	0.01–2.0 μl
Capillary (open tubular): 250 mm inner diameter, 0.2 μm film	0.01–3.0 μl

Zellers and Wise, Najafi, and Aslam.²⁰ Though previous workers have noted that power consumption may be reduced via minimization of the mass of adsorbent, pressure drop across the adsorbent bed, flow rate, and desorption temperature,³ none to our knowledge have performed a theoretical analysis of the factors influencing the power consumption of these microdevices. Many silicon-based microelectromechanical systems (MEMS) besides the device studied here, incorporate heaters (e.g., microsensing devices,²¹ thermomechanical writing and reading process devices,²² microfluidic devices for DNA detection²³ and microgas separation columns⁹). Some reduction in thermal mass, vacuum sealing, and some latitude in selection of locations of heaters can generally be made in these systems. In the present work, we examine, via three-dimensional (3D) finite element modeling, power reductions possible using various strategies in housing and cycling one of the largest power consumers in a μGC device: the preconcentrator.

II. PRECONCENTRATOR

Preconcentrators, or “microtraps,” commonly used in GC systems typically consist of stainless steel cylindrical tubes, lined with silica,^{5,24} though some have been constructed of ioconel 600,²⁵ and glass.²⁶ Typical inner diameters are ~ 0.53 – 1.00 mm, and typical lengths are ~ 100 – 150 mm, and thus typical volumes are approximately 0.012 – 1.35 cm^3 as described in Table II.^{5,14,24–30} Capillary tubes described in Table II, also have disadvantages of large “dead” volume, the interstitial or interparticle volume of the column, and limited heating efficiency, due to their larger thermal mass. In on-line gas chromatography, preconcentrators are used to concentrate analytes and then are heated to desorb the analytes into a narrow plug that is injected into the GC. A microtrap must contain sufficient adsorbent mass (surface area) to ensure quantitative trapping of vapors from the sample stream, but small enough to be rapidly heated to ensure complete desorption and minimize desorbed vapor bandwidth. Hence, fast heating and equally distributed temperature throughout the device are vital for preconcentrator desorption efficiency and bandwidth because rapid desorption is crucial to generate narrow bands for injection into the GC. The rate of desorption is dependent upon both the heating rate of the constituents in the preconcentrator, and the maximum temperature reached in the device.

Preconcentrators are generally heated via direct resistance, because of the near-perfect efficiency attainable in electrical-thermal conversion.³¹ Typically, alternating currents of ~ 5 – 10 A at relatively high voltages of ~ 20 – 50 V are required to heat a preconcentrator. The heating rate, operation time, and maximum temperatures achieved depend on the size, shape, and material used for the preconcentrator, mobile gas, type of adsorbent, and type of analysis as illustrated in Table II.^{1,8,28} For a sufficiently narrow band injection, the temperature distribution throughout the bed must be consistent.

Given the very short heating times and rapid changes in temperature required of the device, determination of the temperature profile within a preconcentrator is a nontrivial experimental exercise. Conventional thermocouples provide excellent accuracy, having capability to determine temperatures within ~ 0.2 $^{\circ}\text{C}$ and reliable resolution in detection of 0.01 $^{\circ}\text{C}$.³² They lack, however, the subsecond response times needed to allow tracking of the effects of the high-speed heating and cooling cycles within these devices. High-speed infrared cameras are also commonly used to determine temperature distribution, but they offer only surface measurements.³² Thus, in this study, we perform 3D finite element simulations of heat transfer, given the difficulty in determining temperature distributions experimentally.

To design for low power, and rapid, consistent heating of the preconcentrator, several factors were examined: the heat transfer mechanisms—conduction, convection, or radiation; effects of contact pad placement, size and location; thermal mass reduction of preconcentrator housing; packaging, and a stop-flow^{5,33} technique that allows for the heating of the preconcentrator device before power losses due to convection can be accumulated. For specificity in our 3D finite element models, we analyzed a preconcentrator microtrap device, which is the successor to the single stage preconcentrator fabricated by Tian *et al.*^{16,34} Our device, top and side views depicted in Figs. 1(a) and 1(b), are larger than the previous-generation version (with a total volume of ~ 11.7 μl as opposed to a volume of ~ 5.6 μl) in the single-stage version studied by Tian *et al.*³⁴ Our device consists of a silicon microheater packed with granular adsorbent used for the capture and concentration of vapors from the environment for subsequent focused thermal desorption and transport to a μGC system. The larger size of this preconcentrator allows for three types of adsorbent instead of one, having higher selectivity due to the higher surface area. Commercial materials, including (in order of increasing surface area) Carbo-pack B, Carbo-pack X, and Carboxen 1000, have been proposed as the sorbents, where a staging strategy is used to entrap more volatile compounds using higher surface area materials, during the injection phase. The preconcentrator operation can be summarized as follows:

- (1) Sample collection stage. Air—the carrier gas and sample flows through the preconcentrator at a rate of 25 cm^3/min , is adsorbed, i.e., accumulated on the surface of the adsorbent beads over a 10 min duration of time.

TABLE II. Preconcentrator/microtraps used from 1993 to 2003.

Workers	Year	Description of Concentrator	Temperature, Current and Power Requirements	Components Analyzed
E. T. Zellers, M. Morishita, Q.-Y. Cai	2000	<ul style="list-style-type: none"> 2 cm in length CuNi sleeve fashioned to encapsulate the two types of trap for rapid thermal desorption two types porous layer open tubular (PLOT) traps: PLOT-Q o.d. = 0.635 mm, i.d. = 0.432 mm and 1 cm long PLOT-S o.d. = 0.935 mm, i.d. = 0.671 and 1 cm long 	<ul style="list-style-type: none"> Heated to 200-205 C less than or equal to 2 s, and cooled to about 70C within a few seconds of switching off the heater power 6 volts used to resistively heat trap 	2-butanone, trichloroethylene, toluene, and m-xylene
S. Mitra, C. Feng, L. Zhang, W. Ho, and G. McAllister	1999	<ul style="list-style-type: none"> Silica lined stainless steel tube with Carbotrap C used for adsorbent o.d. = 0.53 mm and length = 15 cm 	<ul style="list-style-type: none"> resistively heated to temperatures between 250-400 C by a short pulse 0.8 - 1.2 s 7 - 10 A current provided 	butane-2-one, hexane, benzene, toluene, and trichloroethane
W. Chen, Y. H. Xu, and S. Mitra	1998	<ul style="list-style-type: none"> two silica lined stainless steel tube microtraps used: 0.53 mm = i.d. and 9 cm in length and second was 1.5 mm = i.d. with length of 5 cm smaller microtrap used 60 mesh Carbotrap C as the adsorbent and the larger used 20-40 mesh Carbotrap C for the adsorbent 	<ul style="list-style-type: none"> information was not provided 	benzene, toluene, TCE, and ethylbenzene
C. Feng and S. Mitra	1998	<ul style="list-style-type: none"> Used two traps of different size in series and operating sequentially Were made in two i.d.s = 1.1 and 1.3 mm packed with 0.4 and 0.8 g of adsorbent - 10 cm long Smaller diameter trap - retention trap where analytes are desorbed and focused were made with i.d. = 0.53 mm i.d. packed with 0.02 g of sorbent - 10 cm in length Carbotrap C was used as adsorbent and 6.0 mL/min was flow rate of sample 	<ul style="list-style-type: none"> temperature range between 350 and 400C 	methanol, acetone, 1-propanol, and 2-butanone
R. A. Ketcha, C. Gron, and F. R. Lauritsen	1998	<ul style="list-style-type: none"> stainless steel tube or glass tube used for the microtrap, i.d. = 4.5 mm, o.d. = 6.1 mm, and length = 85 mm 22 - 120 mg of adsorbent was used, Tenax TA 60/80 mesh, Tenax GR 60/80 mesh, HayeSepD 80/100 mesh, Chromosorb 105 60/80 mesh or Silica gel 60 70-230 mesh 	<ul style="list-style-type: none"> resistively heated at a rate of 10 - 100 C/min, 30 - 300 C max. temperature 	trans-1, 2-dichloroethene, chloroform, carbon tetrachloride, trichloroethene, toluene, tetrachloroethene, xylenes, styrene, and 1, 2-dibromo-1, 2-dichloroethene
N. Zhu, Z. Li, and S. Mitra	1997	<ul style="list-style-type: none"> 0.53 mm i.d., length 15 cm deactivated fused-silica lined stainless steel tubing with commercial adsorbent, Carbotrap C carrier gas = nitrogen 	<ul style="list-style-type: none"> temperature and power not mentioned 	benzene, acetone, toluene
S. Mitra, N. Zhu, X. Zhang, and B. Kebbekus	1996	<ul style="list-style-type: none"> 0.53 mm i.d. deactivated fused-silica-lined stainless-steel tube, length was about 147 cm with Carbotrap C used for adsorbent 	<ul style="list-style-type: none"> resistively heated so 300C could be reached within 1 - 2 s pulses of current between 7 - 10 A 	benzene, trichloroethylene, toluene, and ethylbenzene
S. Mitra, Y. H. Xu, W. Chen, and A. Lai	1996	<ul style="list-style-type: none"> silica lined stainless steel tubing, i.d. = 0.53 mm and 10-14 cm long with an adsorbent = Carbotrap carrier gas = nitrogen with flow rate from 4.76 ml/min to 10.34 ml/min 	<ul style="list-style-type: none"> resistively heated with 20-50 volt AC temperature range between 344.8 - 416.67 K 	1 ppm each of benzene, toluene, ethylbenzene, and trichloroethane, along with combustion products C ₂ , CO, SO ₂ , and O ₂
Y. H. Xu and S. Mitra	1994	<ul style="list-style-type: none"> silica lined stainless steel tube length of 14 cm and i.d. = 0.52mm with 60 mesh (0.25 mm) carbotrap C as adsorbent 	<ul style="list-style-type: none"> resistively heated by 5-10 A current for a duration of 500 to 1500 ms. microtrap resistance = 0.1W/cm microtrap connected to a variable power supply 20-50 volt AC 	toluene, ethylbenzene, benzene, dichloromethane, tichloroethane, acetone, ethanol
S. Mitra and C. Yun	1993	<ul style="list-style-type: none"> stainless-steel tubing, i.d. = 0.33 mm and adsorbent = Carbotrap flow rates in microtrap were between 4.7 and 8.1 mL/min 	<ul style="list-style-type: none"> resistively heated with current between 5 - 10 A for 100 - 1000 ms temperatures as high as 300C reached 	benzene, toluene, xylene, p-Xylene

Workers	Year	Description of Concentrator	Temperature, Current and Power Requirements	Components Analyzed
I. Ciucanu, A. Caprila, A. Chiriac, and R. Bama	2003	<ul style="list-style-type: none"> Silicosteel capillary tube with helical sorbent fixed inside of tube sorbent - helical structure made by wrapping with a constant pitch a 0.07 mm diameter chromium-aluminum alloy wire, coated with 0.05 of PDMS i.d. = 0.75 mm, o.d. = 0.95 mm, and length = 80 mm carrier gas = hydrogen at 5 mL/min 	<ul style="list-style-type: none"> 260 C @ 17 V for 1-2 ms 200 C at 10 V for 10 ms resistively heated 	benzene, trichloroethylene, toluene, tetrachloroethylene
M. Kim and S. Mitra	2003	<ul style="list-style-type: none"> Microfabricated preconcentrator etched on 6 inch silicon wafer using standard photolithographic techniques 20-50 can be placed on a single wafer Several channel configurations fabricated with widths between 50 and 456 μm with depths between 35 and 350 μm, and lengths between 6 and 19 cm OV17 (50% polymethyl-50% phenyl phase) were deposited on the microconcentrator by spin coating for formation of an adsorbent layer carrier gas = nitrogen 	<ul style="list-style-type: none"> 200 C could be reached in less than 10 s resistively heated 	benzene, toluene, and xylene
J. M Sanchez and R. Sacks	2003	<ul style="list-style-type: none"> Inconel 600 (Ni-Co alloy) tube with 4 different carbon based adsorption materials (2.2 mg of each material used) i.d. = 1.35 mm and 80 mm in length flow rate of sample gas through trap ~50-100 cm³/min carrier gas = hydrogen 	<ul style="list-style-type: none"> trap resistively heated to 300C resistance of the trap = 0.48 Ω adjustable AC power provided with use of auto transformers 	Vapor concentrators of 8 - 35 ppm (v/v) were used, 42 volatile compounds spanning a volatility range from n-C ₂ to n-C ₁₂
L. Morris, D. J. Caruana and D. E. Williams	2002	<ul style="list-style-type: none"> Three pieces of machinable ceramic (20X20X6 mm³ each) bolted together, where top and bottom pieces support stainless steel fittings to attach tube trap center piece machined to hold a sorbent bed 6 mm in diameter and 6 mm thick surrounded by a heating coil wound with TA wire Tenax TA 60-80 mesh was used as adsorbent carrier gas = dry air and total flow rate = 100 cm³/min 	<ul style="list-style-type: none"> temperature range of trap = 200-220 C resistively heated 	heptane, toluene, octane, xylene, nonane, propylbenzene, methylstyrene, phenol, and cresol
D. Kou, A. San Juan, and S. Mitra	2001	<ul style="list-style-type: none"> silica lined metal tube packed with 0.02 g of Carboxpack C o.d. = 0.53 mm and 15 cm long carrier gas = nitrogen at a flow rate of 1 mL/min 	<ul style="list-style-type: none"> resistively heated 7-10 A current supplied 30 volt AC power source 	benzene, toluene, and ethylbenzene
C.-J. Lu and E. T. Zellers	2001	<ul style="list-style-type: none"> Two preconcentrators used: thin walled glass capillaries (1.15 mm i.d., 1.70 mm o.d.) and length of 7.5 cm, mass of adsorbent packed into tube ranged from 1 to 10 mg, larger preconcentrators used = 1.80 mm i.d. and 0.051 mm wall same length, but larger mass of adsorbent used adsorbents examined: Carboxen 1000, Carboxpack X, Carboxpack B, Tenax TA, and Tenax GR 	<ul style="list-style-type: none"> temperature range = 180 - 400C resistively heated 	20 VOCs from seven different chemical classes that span a vapor pressure range from 8 to 231 Torr, examples: acetone, 2-propanol, benzene, toluene, m-xylene, and p-xylene, etc.
I. Ciucanu and J. Pawliszyn	2001	<ul style="list-style-type: none"> Stainless steel tubing with sorbent was Tenax-TA i.d. = 0.5 mm, o.d. = 0.65 mm, and 60 mm long carrier gas = hydrogen of the metal tubing for some milliseconds by discharging a 17 mF capacitor. Trapping time is 40 seconds and entire system powered by a 12 Volt DC car battery. The trap from Supelco (Mississauga, ON, Canada). 	<ul style="list-style-type: none"> Entire system power by 12 volt DC trap resistively heated with 17 mF capacitor 	benzene, toluene, ethylbenzene, trichloroethylene, tetrachloroethylene, α -pinene, and limonene
C. Feng and S. Mitra	2000	<ul style="list-style-type: none"> Silica stainless steel tubing and adsorbents used: Carboxieve SIII, Tenax-TA and Anasorb 747 Two traps used: 0.53 mm i.d., 0.78 mm o.d., and 10 cm long; and 1.1 mm i.d., 1.5 mm o.d., and 10 cm long Desorption made by smaller trap by short electrical pulses 1-5 seconds and 3-5 seconds for larger traps 	<ul style="list-style-type: none"> temperature = 440F resistively heated where 296C could be reached either using 5s/60volt pulse or 4s/70 volt pulse 	acetone, methanol, and benzene

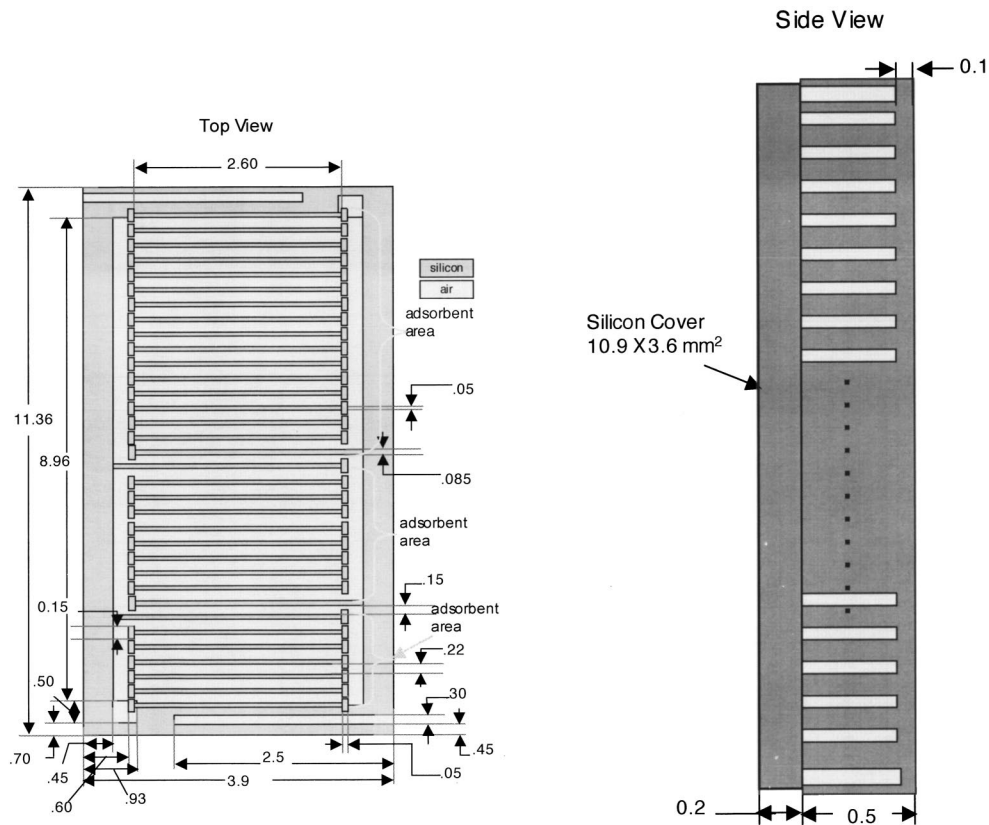


FIG. 1. (a) Top view and (b) side view of preconcentrator design (units in mm).

- (2) Injection stage. Preconcentrator is resistively heated via application of direct current from a wire and organic compounds are desorbed as a concentrated plug due to the sharp increase of temperature to 275 °C, within 12 s.
- (3) Desorption stage. Analyte is expelled from the preconcentrator into the columns, at a flow rate of $\sim 1.5 \text{ cm}^3/\text{min}$.

Tian *et al.*,³⁴ through experiments on a single stage preconcentrator containing only one type of adsorbent bead, with a smaller sample volume demonstrated that the power consumption of a single stage 520- μm -thick Si microheater could be reduced from 1.05 W at 250 °C, atmospheric pressure, to 0.675 W at 1.2 Torr, representing a reduction of $\sim 35\%$ in total heating power. They also illustrated that the size of air gaps around the microheater (thermal isolation) affected experimental heating rates achievable in the device; for their device an increase in air gap from 100 to 500 μm increased the heating rate by 50%.

Here, we examine the specific relation of these, and several additional design parameters, including use of the stop-flow technique,^{5,33} to reduce power demand. The scale-dependent and relative influences of contact pad location and size, device external surface area, volumetric air flow rate, and system thermal mass were specifically examined. We also examine how the preconcentrator power profile, power consumption versus time, relates to the selection of power supply for μGCs used for the analysis of semivolatile and

volatile organic compounds. For example, Tian *et al.*³⁴ suggested optimization of stop-flow time and resulting preconcentration factor, for minimization of total power consumption, constrained by a minimum injection volume required. However, as we will show here, consideration of power density is an additional important factor, since rapid temperature ramp times necessitate correspondingly higher power density supplies, which limit the choice of possible power supplies.

III. METHODS

A. Numerical methods and heat transfer model

Simulation conditions were matched to the design goals of the environmental monitor of the University of Michigan Center for Wireless Integrated Microsystems (WIMS) (Fig. 2).²⁰ Specifically, gases within the preconcentrator were

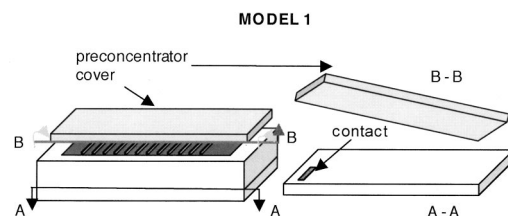

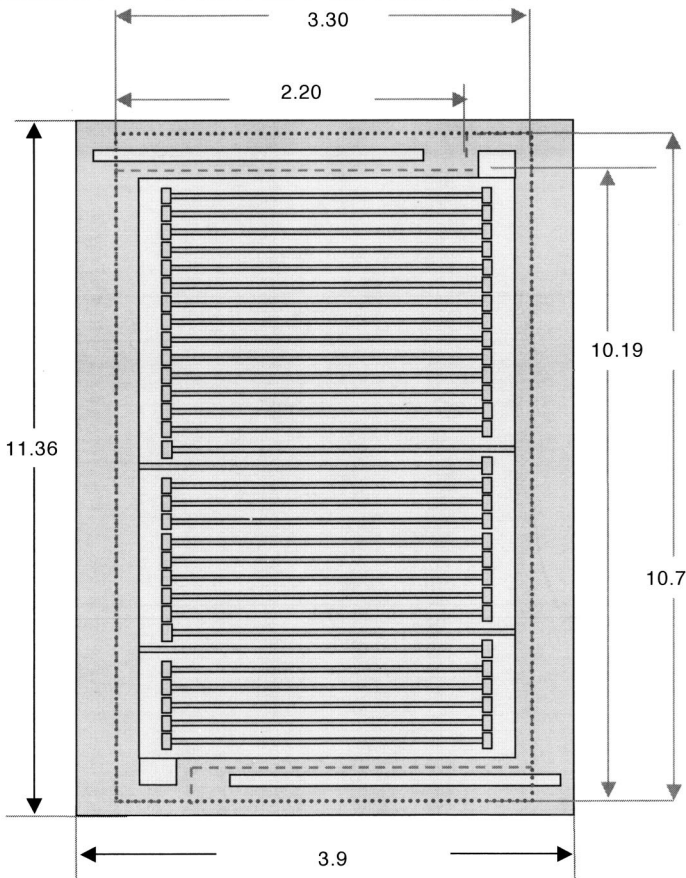


FIG. 2. Schematic of preconcentrator reference geometry and contact pad location—Model 1.

TABLE III. Preconcentrator geometries used in finite element analyses (units in mm).

Geometry	Description of Preconcentrator Geometry	Illustration
A	Control (reference) - 11.36 X 3.9 X .7 mm ³ volume 	
B	Reduction of control volume by 17.47% by elimination of silicon material along outer ring of device (material outside of red dotted line removed) ● ● ● ● ●	
C	Reduction of control volume by 23.98% by elimination of silicon material along outer ring of device (material outside of red dotted line removed) ■ ■ ■ ■ ■	

heated to an average temperature of 275 °C within 3 s, and held at this temperature for 10–12 s. The maximum and minimum allowable temperatures in the preconcentrator were specified as 300 and 235 °C, respectively. Detailed descriptions of preconcentrator geometries and models are provided in Tables III–V respectively.

Finite element simulations of transient heat transfer within the preconcentrator were run using ABAQUS.³⁵ Although a heat transfer analysis was performed, heat transfer governing equations are obtained using those analogous to those employed in stress analysis, i.e., those used to determine continuum displacement.³⁶ All analyses were transient, so heat capacity effects could be included in analyses of the rate of heat generation. Because of the small areal footprint of the contact pad relative to the size of the device, instantaneous equilibration in the contact pad was assumed during heating. The direct resistance heating of the preconcentrator was thus modeled by applying a known heat flux per unit area to a defined number of elements comprising the areal footprint of the contact pads, delivered by current-carrying wires. The initial temperature for all nodes was set to 25 °C.

Heat flux was equally distributed over the surface area of the contact pad region (e.g., 0.61 mm² for Model 1). The preconcentrator is heated by joule heating: a current-carrying wire is attached directly to contact pads on the device. Here we modeled the contact pad with a layer of elements having identical areal footprint to the actual contact pads, 0.61 mm².

We did not mesh the current-carrying wires, since wires are required for any preconcentrator design where Joule heating is used. Though all connects play a role in heat transfer, we limited consideration of design variables to those which would not be obvious targets for reduction; simply, we assumed that in any design considered, the number of connects would already be minimized.

Radiative heat loss was not modeled in any of the preconcentrator simulations; instead, estimates were obtained via

$$\text{Radiation}[W/m^2] = \varepsilon \sigma (T_s^4 - T_{\text{sur}}^4). \quad (1)$$

Specifically, the computed heat loss per second from the surface of the preconcentrator's outer housing due to radiation was approximately ~0.20 W, where T_s and T_{sur} are device

TABLE IV. Case studies examined for analysis of WIMS-ERC preconcentrator design models 1 through 6.

Case studies				
Design change considered	Model number	Description of model	Geometry (detailed in Table III)	Mechanism(s) of heat transfer examined
Reference simulation	1	Control simulation, contact pad surface area=0.61 mm ² seen in Fig. 2.	A	<ul style="list-style-type: none"> • Conduction of air inside of preconcentrator • Adsorbent excluded • No conduction, radiation, or convection external to the preconcentrator, i.e., preconcentrator within a vacuum
Variation of contact pad parameters	2(a)–(c)	Increase of contact pad surface area by a factor of (a) 1.17, (b) 1.42 and (c) 1.93. Detailed in Table V.	A	<ul style="list-style-type: none"> • No conduction, radiation, or convection external to the preconcentrator, i.e., preconcentrator within a vacuum
	2(d) and (e)	Two contact pads are used with equal surface area=0.305 mm ² . Both are located diagonally located wherein, (d) both are on the bottom of the device and (e) one is on the top cover and the other is on the bottom of device. Detailed in Table V.	A	
	2(f) and (g)	Contact pad with surface area=0.61 mm ² is located (f) at the bottom of the device at the center and (g) on a bridge between slat and outer ring of device. Detailed in Table V.	A	
Elimination of silicon from outer ring of device (reduction in thermal mass)	3	Thermal mass of preconcentrator reduced by eliminating silicon from outer ring of the device by 17.5% of volume. Location of contact pad depicted in Fig. 2.	B	
	4	Thermal mass of preconcentrator reduced by eliminating silicon from outer ring of device by 24.0% by volume. Location of contact pad depicted in Fig. 2.	C	
Elimination of vacuum sealing of preconcentrator	5	Convection external to the device added to examine additional losses when no packaging is present. Location of contact pad depicted in Fig. 2.	A	<ul style="list-style-type: none"> • Conduction and natural convection of air inside of preconcentrator • Adsorbent included • Convection external to the preconcentrator included
Introduction of gas dwell in preconcentrator (stop flow)	6	Convection inside of the preconcentrator eliminated while preconcentrator heated during the first 3 s temperature ramp up. Location of contact pad depicted in Fig. 2.	A	<ul style="list-style-type: none"> • Conduction air inside of preconcentrator • Adsorbent included • No conduction, radiation, or convection external to the preconcentrator, i.e., preconcentrator within a vacuum

surface and ambient temperatures of the device, of 275 and 25 °C, respectively, σ is the Stefan–Boltzmann constant, equal to 5.670e-8 W/m² K,⁴ and 0.68 is the emissivity, ϵ , of *n*-silicon (doping concentration=2.94 × 10¹⁴ cm⁻³; thickness=1770 μm). We assumed a wavelength range between 0.4 and 1.0 μm, wherein the emissivity of silicon is nearly independent of temperature and increases from 0.45 to 0.68.³⁸ We did not perform a detailed study in the present work on radiative losses, since they pose a difficult problem in design, i.e., other variables are more easily changed to reduce power. Later, we comment on future work on this

issue, though we do report estimates of radiative losses in all scenarios considered.

The partial differential equation governing transient heat transfer for the three-dimensional region, Ω , and boundary Γ separated into two portions: Γ_1 and Γ_2

$$c \frac{\partial u}{\partial t} - \frac{\partial}{\partial x} \left(k_x \frac{\partial u}{\partial x} \right) - \frac{\partial}{\partial y} \left(k_y \frac{\partial u}{\partial y} \right) - \frac{\partial}{\partial z} \left(k_z \frac{\partial u}{\partial z} \right) + q''' = f(x, y, z, t), \quad (2)$$

was solved numerically, with boundary conditions

TABLE V. Description of contact pad variability in size and location and simulation results for models 1 and 2(a)–2(g).

Simulation description	Power Saving or [Loss] Compared to Model 1 (a)	Bead Bed ΔT ($T_{\max} - T_{\min}$)%	Location of Contact Pad
Model 1 – Reference simulation (contact pad area = 0.61 mm ² , heat flux = 2.459 W/mm ²)	NA	5.1	
Model 2 (a) Contact pad surface area increased by 1.17 (contact pad area = 0.715 mm ² , heat flux = 2.098 W/mm ²)	0%	5.1	
Model 2 (b) Contact pad surface area increased by 1.42 (contact pad area = 0.869 mm ² , heat flux = 1.726 W/mm ²)	0%	4.9	
Model 2 (c) Contact pad surface area increased by (contact pad area = 1.177 mm ² , heat flux = 1.274 W/mm ²)	0%	4.7	
Model 2 (d) Two contact pads – both pads located at the bottom (each contact pad area = 0.305 mm ² , heat flux per pad = 4.918 W/mm ²)	0%	4.8	
Model 2 (e) Two contact pads - one on the top cover and other on the bottom, offset at a diagonal (each contact pad area = 0.305 mm ² , heat flux per pad = 4.918 W/mm ²)	0%	2.9	
Model 2 (f) One contact pad located at the center of the preconcentrator (contact pad area = 0.61 mm ² , heat flux = 2.459 W/mm ²)	0%	2.9	
Model 2 (g) One contact pad located on the bridge between the outer ring and slat (contact pad area = 0.61 mm ² , heat flux = 2.459 W/mm ²).	[0.13%]	5.2	

$u = \hat{u}$ on Γ_1 and $q_n = \hat{q}_n$ on Γ_2 , where

$$k_x \frac{\partial u}{\partial x} n_x + k_y \frac{\partial u}{\partial y} n_y + k_z \frac{\partial u}{\partial z} n_z = \hat{q}_n, \quad (3)$$

c is the heat capacity, k_x , k_y , k_z are the thermal conductivity of the material in directions x , y , and z respectively, u defines the known surface temperature, and q''' is the rate of heat generated per unit volume, and t denotes time. Initial conditions ($t=0$) are given by $u(x, y, z, 0) = u_o(x, y, z)$ in Ω . The weak form of the governing equation and the boundary condition equations over an element Ω^e is obtained by multiplying Eq. (2) by a weight function $v(x, y, z)$ and integrating over the element using the divergence theorem, per

$$0 = \int_{\Omega^e} \left[v \left(c \frac{\partial u}{\partial t} + q''' - f \right) + k_x \frac{\partial v}{\partial x} \frac{\partial u}{\partial x} + k_y \frac{\partial v}{\partial y} \frac{\partial u}{\partial y} + k_z \frac{\partial v}{\partial z} \frac{\partial u}{\partial z} \right] dx dy dz - \oint_{\Gamma^e} q_n v ds. \quad (4)$$

The resulting semidiscrete finite element model in matrix form

$$[M^e] \{\dot{u}^e\} + [K^e] \{u^e\} = \{f^e\} + \{Q^e\}, \quad (5)$$

where M^e is the mass matrix, K^e is a matrix containing constants pertaining to conductance and convection, f^e is the

vector pertaining to generation of heat per unit volume, Q^e is a vector corresponding to the heat flow into and/or out of the element, and u^e represents the temperature vector, where

$$M_{ij}^e = \int_{\Omega^e} c \psi_i \psi_j \times dx dy dz. \quad (6)$$

$$K_{ij}^e = \int_{\Omega^e} \left(k_x \frac{\partial \psi_i}{\partial x} \frac{\partial \psi_j}{\partial x} + k_y \frac{\partial \psi_i}{\partial y} \frac{\partial \psi_j}{\partial y} + k_z \frac{\partial \psi_i}{\partial z} \frac{\partial \psi_j}{\partial z} + q''' \psi_i \psi_j \right) \times dx dy dz. \quad (7)$$

We assume the heat generation term, f^e is zero.

A sample mesh, used for nearly all simulations, is shown in Fig. 3; the absence of any system symmetries necessitated full, 3D simulation. Meshes were comprised of eight-noded continuum displacement, three-dimensional (DC3D8) elements.

B. Material properties

The adsorbent, spherical carbon beads within the preconcentrator were modeled as a lumped mass. Effective thermal conductivity, K_m , was determined following Rayleigh's classical expression³⁹ for the effective conductivity of a cubical lattice of spheres in air, per

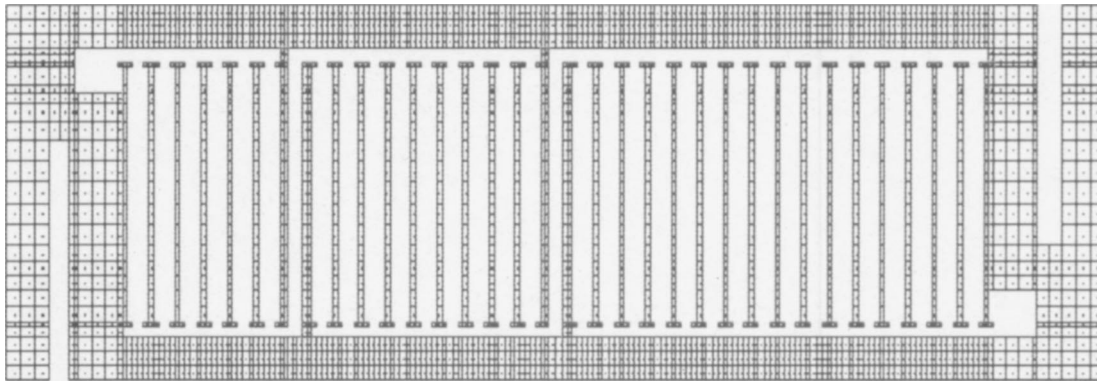


FIG. 3. Top view of the finite element mesh, specifically of the outer ring and slats of the preconcentrator.

$$K_m = 1 - \frac{3f}{\frac{2 + K_d}{1 - K_d} + f - \frac{0.525(1 - K_d)f^{10/3}}{\left(\frac{4}{3} + K_d\right)}}, \quad (8)$$

where K_d and K_m are normalized graphite and effective conductivities, respectively, relative to medium conductivity K_c , i.e.,

$$K_d = \frac{k_d}{k_c}, \quad (9)$$

and

$$K_m = \frac{k_m}{k_c}. \quad (10)$$

Values K_d and K_c , the particle and medium conductivities, were estimated to be $1.67e-1$ and $2.51e-5$ W/mm K, and were used to solve for K_m . The specific heat of the adsorbent bed mass was calculated via

$$C_{p\text{-mix}} = \frac{\bar{C}_{p\text{-mix}}}{MW_{\text{mix}}}, \quad (11)$$

where MW_{mix} is the molecular weight of the mixture

$$\bar{C}_{p\text{-mix}} = \frac{1}{n_{\text{total}}} \sum_i (n_i c_{pi} + n_s c_s) \quad (12)$$

and n_{total} is the total number of moles, n_s is the number of moles of solid, n_i is the number of moles of gas, c_s is the specific heat of solid, and c_{pi} is the specific heat of air. Material properties used in the analyses are summarized in Table VI.

Convective losses among particle beads were not computed; the bead bed was modeled as a composite material of graphitic particles in air. Laminar flow within the packed column was assumed. The coefficient of heat transfer was calculated for channels in the device exposed to air. The heat transfer coefficient for laminar tubular flow in a channel with friction factor f , length L , and hydraulic diameter D_h , is given by

$$h_L = f \frac{L}{D_h} \frac{V^2}{2g_c}, \quad (13)$$

where

$$f = \frac{64}{\text{Re}} \quad (14)$$

and

$$D_h = \frac{4A}{P} \quad (15)$$

and A is the cross sectional area of the duct, P is the perimeter of the duct, V is the average velocity of the fluid within the duct, and Re is Reynold's number. The proportionality constant g_c is 1 kg m/Ns^2 , in SI units.

For Model 5, natural convection of air along the surfaces of the outside walls of the preconcentrator was assumed. The heat transfer coefficient, \bar{h} , for free flow over a flat plate can be derived using the Nusselt number. For any flat plate with a characteristic length, L , Nu_L is

$$Nu_L = \frac{\bar{h}L}{k}, \quad (16)$$

where

$$\bar{Nu}_L = \left\{ .825 + \left[\frac{.387Ra_L^{1/6}}{1 + \left(\frac{.492}{Pr}\right)^{9/16}} \right]^{8/27} \right\} \quad (17)$$

for a vertical plate, and

TABLE VI. Material property values used in finite element analyses.

Material	Density (kg/mm ³)	Thermal conductivity (W/mm K)	Specific heat (J/kg K)
Silicon	2.33e-06	1.26e-01	7.03e02
Glass—silica	2.20e-06	1.38e-03	7.45e02
Graphite	2.25e-06	1.67e-01	7.07e02
Air	1.29e-09	2.51e-05	1.00e03

$$Nu_L = .54Ra_L^{1/4} \quad (18)$$

for a horizontal plate.³⁷

In Eqs. (17)–(19), Ra_L and Pr are the Randel numbers, respectively, for air at a given state. Ra_L is determined from

$$Ra_L = \frac{g\beta(T_s - T_\infty)L^3}{\nu\alpha}, \quad (19)$$

where g is 9.81 m/s^2 , β is the volumetric thermal expansion coefficient, T_s is the surface temperature of the air, of $275 \text{ }^\circ\text{C}$, T_∞ is the ambient temperature of $25 \text{ }^\circ\text{C}$, L is the characteristic length, ν is the kinematic viscosity of air, and α is thermal diffusivity. All of the properties used were taken at the film temperature, T_f , of

$$T_f = \frac{T_s + T_\infty}{2}. \quad (20)$$

The characteristic length, L , is equal to the length of the plate for vertical plate calculations, and A_s/P , for a horizontal plate, where A_s is the surface area of the plate and P is the perimeter of the plate, as explained in the following sections.

The preconcentrator was fabricated from $\langle 100 \rangle$ p -type silicon and contact areas were constructed as thin oxide/nitride/oxide layers. All properties selected for silicon were taken for pure silicon at a reference temperature of $25 \text{ }^\circ\text{C}$, since the other species were of low overall content (less than $10^{16} \text{ atoms/cm}^3$,^{40,41} and low contact resistance was assumed.⁴² Conductivity (1.26e-1 W/mm K) and specific heat (7.03e2 J/kg K) were used, since thermal conductivity is nearly independent of dopant concentration for temperature above 100 K .⁴³ Constant thermal conductivity and specific heat were assumed in all simulations.

C. Case studies

The purpose in modeling the preconcentrator was to determine the power versus time profile required to heat the preconcentrator to $275 \text{ }^\circ\text{C}$ within 3 s , and maintain this temperature for 9 s . The input power required to achieve this temperature was trial and error: increasing heat flux rates were specified until $275 \text{ }^\circ\text{C}$ was achieved. The required power input was the variable under investigation, hence, each point in power versus time profiles represents one or more simulations.

Our studies were performed using a design that is the successor to an earlier version studied by Tian *et al.*^{16,34} This larger device has a total volume of $\sim 11.7 \mu\text{l}$, increased from the volume of $\sim 5.6 \mu\text{l}$ in the single-stage version studied by Tian *et al.*^{16,34} Tubular preconcentrators are typically heated to hundreds of degrees within a fraction of a second,⁸ and thus both short heating times and uniformity of temperature are important, and were studied here.

We examined four different strategies for power reduction in the preconcentrator. First, variations in contact pad size and configuration were considered (Table V), to quantify the amount of time and power required to heat the device. Second, the effects of thermal mass reduction of the silicon preconcentrator housing were studied (Table III). Third, a pack-

aging study was conducted to examine power savings by addition of top and bottom-mounted device covers to allow vacuum sealing, which would reduce heat losses (Table IV). Fourth, a stop-flow technique^{5,33} for heating the preconcentrator conductively was performed, to study whether reduction in convective losses in the preconcentrator would reduce power demand, via elimination of convective losses (Table IV).

A total of five models were used to examine the heat transfer in the device; Model 1 was used as the reference configuration. Table III shows the geometries of all models for analysis of the WIMS ERC three-stage preconcentrator; Tables IV and V include listings of the individual case studies performed. Models 1 and 2(a)–(g) were used to examine the effects of variation of contact pad size and location. Models 3 and 4 were used to examine the effects of reduction of thermal mass on the power consumption of the preconcentrator. Model 5 was used to examine the power savings resulting from vacuum packaging of the preconcentrator, and Model 6 was used to examine the power consumption benefits resulting from use of the *stop-flow*^{5,33} technique. The volumetric air flow rate through the preconcentrator was chosen to be $1.5 \text{ mm}^3/\text{min}$. All simulations (Models 1 and 6), except for the packaging study (Model 5) assumed the system to be vacuum sealed, hence neither conduction nor convection external to the device was considered in these simulations. Simulation times reflected the 12 s operation time of the real device. No external components to the preconcentrator were modeled. For all models wherein forced flow was applied, the mobile gas flow was assumed to be laminar, given the low Reynold's numbers typically associated with such flows.⁴⁴

1. Alterations in contact pad geometry/location

The actual preconcentrator has two contact pads; current is supplied to one contact pad via a wire, while the other contact pad is used to ground the device. The reference configuration, Model 1 (Fig. 2), had only a single contact pad of area 0.61 mm^2 , located on the lower left-hand side of the bottom of the preconcentrator, since direct resistive heating is assumed. Heat was delivered to the preconcentrator through the contact pad surface, and thus Q^e in Eq. (5) is nonzero only for elements within the surface area of the contact pad region. No beads were included in this case study. Also, heating was assumed to be conductive, and therefore in Eq. (7), all k_o terms for convection external to the preconcentrator are set to zero to reflect zero convective heat transfer.

Geometry A, shown in Table III, and contact pad variations in location and size were modeled as indicated in Table V. In all of the cases (Table V) the peak power was 3.70 W and the sustained power was 0.65 W . Alterations in the locations and/or sizes of contact pads appeared to have no significant effect on required heat flux, though they did produce changes in initial temperature distribution (within 1 s), which may be important for the chemical sensing functionality. Specifically, average bead bed temperatures for simu-

TABLE VII. Summary of simulation results for models 1, 3, 4 and 5.

Simulation description	Peak power (J/s)	Sustained power (J/s)	Power saving or [Loss] compared to model 1 (a)
Model 1—Reference simulation	3.70	0.65	NA
Model 3—Elimination of silicon from outer ring of device (reduction in thermal mass)	3.01	0.62	8.12%
Model 4—Elimination of silicon from outer ring of device (reduction in thermal mass)	2.63	0.58	15.31%
Model 5—Elimination of vacuum sealing of preconcentrator	4.38	1.76	[51.18%]
Model 6—Introduction of gas dwell in preconcentrator (stop flow)	3.40	0.65	2.03%

lations where contact pad surface area was systematically increased by factors of 1.17, 1.42 and 1.93, respectively (0.715, 0.869, and 1.177 mm² and input heat fluxes of 2.459, 2.098, 1.726, and 1.274 W/mm², respectively) were within 0.1% of those of the reference configuration, so we omit plots of temperature distribution in these cases. Likewise, average bead bed temperature values for simulations where the contact pads were located in different areas on the surface of the device or in multiple places (two places instead of one) on the device were also nearly identical to Model 1. The maximum difference in average temperature ($T_{\text{avg,Model1}} - T_{\text{avg,Model2}}$) between Model 1 and Models 2(a)–(g) was less than 1%. Temperature variability within bead bed ($T_{\text{max}} - T_{\text{min}}$) for Models 1 and 2(a)–(g) was less than 5.5% (Table V).

2. Elimination of silicon from outer ring of device (reduction in thermal mass)

To quantify the effect of thermal mass reduction on power demand, two separate configurations, Geometry B and Ge-

ometry C (Table III) were constructed, having reductions in silicon volume of 17.5% and 24.0%, respectively, in Models 3 and 4. Areas outside of the dashed lines are eliminated silicon volume. Each contained a single contact pad, of identical location and size to that in Model 1 (Fig. 2).

The components of the preconcentrator modeled in these case studies included the microheater, adsorbent beads, and air; Eqs. (8)–(12) were used to compute effective lumped mass values for specific heat and thermal conductivity for the air and adsorbent beads within the preconcentrator using values shown in Table VI. Both convective and conductive heat transfer were considered, and thus in Eq. (7), k_x (where $x = 1, 2, 3$) and q_n , respectively, were nonzero, to account for conduction among silicon, air and beads, in addition to convection from surfaces of beads, silicon walls and slats.

Reduction in thermal mass resulted in modest power savings. Specifically, the configurations of Models 3 and 4 resulted in a total power reduction of 8.12% and 15.31%, respectively, over a 12 s time interval, as compared to Model 1 (Table VII). Excessive removal of silicon could create struc-

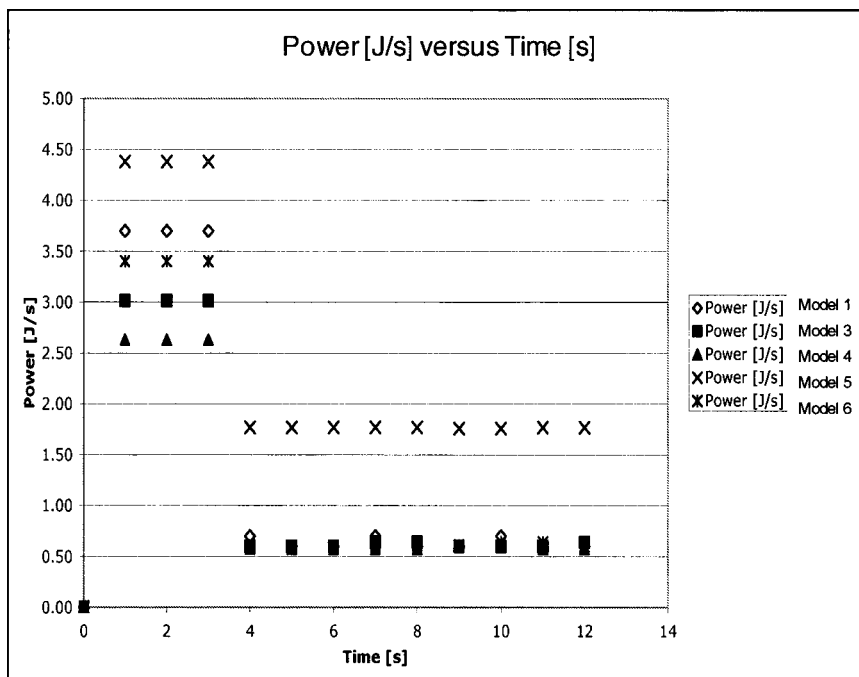


FIG. 4. Power vs time plots for Models 1, 3, 4, 5 and 6.

tural problems with the device; thus examination of replacement of graphite beads with materials of lighter weight (e.g., higher porosity), may be merited.

3. Packaging study (elimination of vacuum sealing of preconcentrator)

A single model was constructed to examine heat losses and attendant increase in power requirements with elimination of vacuum sealing. This configuration, Model 5, again followed Geometry A for contact pad size and location. Beads and air were included in the analysis, and both conductive and natural free convective losses from the external faces of the preconcentrator were examined; in Eq. (7), non-zero terms thus included k_x (where $x=1,2,3$) and q_n to account for conduction between silicon, air and beads, and convection from the surfaces of beads and silicon walls and slats, respectively. As before, effective lumped mass values of specific heat and thermal conductivity for the air and adsorbent beads were used.

Simulation results predict a 51% increase in power consumption (Table VII) over a 12 s interval for the preconcentrator when the vacuum seal is removed, which is comparable to the 35% reduction reported by Tian *et al.*³⁴ for the operation of their smaller microheater (which did not include adsorbent beads and a preconcentrator top). A power versus time profile for the nonpackaged simulation and the packaged simulation are shown in Fig. 4.

Since air must be allowed to flow through the preconcentrator during operation, a complete vacuum seal of the entire device is not a practical option. Two separate seals, however (top/bottom), could be designed. A disadvantage of including a vacuum seal on the top and bottom covers of the preconcentrator is cost, as packaging is one of the most costly parts of microsystem manufacturing, and it is also often the first to fail or negatively influence the system response.⁴⁵ However, uses of other vacuum seals have generally proven effective in other MEMS devices.^{46,47}

4. Introduction of gas dwell in preconcentrator (stop flow)

Introduction of a gas dwell in the preconcentrator, or stop flow^{5,33} involves heating the preconcentrator device to 275 °C within 3 s before pumping air into the preconcentrator. The convective losses are thus eliminated during preconcentrator heating, resulting in power savings. A single case study, Model 5, was used to quantify power reduction, using Geometry A, with contact pad size and location again following Model 1.

Thus, during the 3 s preconcentrator heating time, the portion of the term q_n , relating to convection in Eq. (7) was set to zero, while the conduction terms $k_x(x=1,2,3)$ were nonzero. Convective heat transfer was assumed, once gas was pumped into the preconcentrator.

Use of the stop-flow^{5,33} technique resulted in a 2.03% reduction in power consumption, as illustrated in the power versus time profile of Fig. 4.

IV. RESULTS AND DISCUSSION

As the largest consumer of power in the WIMS ERC μ GC, design of the preconcentrator is critical. Our goal in simulations was to achieve an internal preconcentrator temperature of 275 °C within 3 s, with nearly uniform temperature distribution within the bead bed, while identifying designs that minimized power requirements.

Overall, our simulation results were in general agreement with published experimental values. Model 1, for example, predicts a peak and sustained power demands of 3.70 and 0.65 W, respectively, to achieve a preconcentrator temperature of 275 °C within 3 s, at a flow rate of 1.5 cc/min. Tian *et al.*³⁴ found experimentally that their smaller preconcentrator (lateral dimensions of 3 μ m by 3 μ m, and bed depth of \sim 520 μ m), fabricated using similar techniques as the ones described, produced a target desorption temperature of 275 °C at 5 °C/s with an input power of 1.33 W within 42 s and 15 °C/s with an input power of 2.25 W within 15 s.

Our computational models were designed to be conservative in predicting power demand. We modeled the housing of the preconcentrator as silicon, i.e., 0.50 mm of silicon without the \sim 2.3 μ m film layer. The structure was actually constructed from a *p*-Si wafer, coated with several layers: 0.5- μ m-thick thermal oxide layer, followed by an oxide/nitride/oxide film (0.1/0.1/0.6 μ m thick), 0.5- μ m-thick poly-Si layer, and a 1.0 μ m layer of poly-Si for an adhesion layer for the glass/metal/Si bonding for contact pads.³⁴ Doped polysilicon has lower thermal conductivity values than single crystal doped with comparable concentrations at all temperatures.⁴¹ The concentration of dopant, however, was low in the actual system, and data of Asheghi *et al.*,⁴⁰ and indicate that for temperatures greater than 173.15 °C thermal conductivity is practically independent of the doping level, i.e., at room temperature, thermal conductivity approaches the same value for doped silicon layer, undoped single crystal layer, and undoped single crystal bulk.⁴¹ We did not account for variation of the thermal conductivity of single crystal silicon with temperature, however; for high purity Si, thermal conductivity should decrease somewhat as temperature increases. Also, thermal contact resistance at the metal/electrical insulator interfaces increases the total resistance at the location of the contact pad, and hence generate Joule heating.⁴²

All simulation results are summarized in Tables V and VII; in the following sections, we detail model results for each case study. For comparison, we used the following expression for weighted Power savings/loss, S ,

$$S = \left[\frac{P_p(\text{Model1}) - P_p(\text{ModelA})}{\text{MAX}[P_p(\text{Model1}; \text{ModelA})]} \right] \frac{3 \text{ s}}{12 \text{ s}} + \left[\frac{P_s(\text{Model1}) - P_s(\text{ModelA})}{\text{MAX}[P_s(\text{Model1}; \text{ModelA})]} \right] \frac{9 \text{ s}}{12 \text{ s}}, \quad (21)$$

where P_p is peak power, P_s is the sustained power, and Model A encompasses Models 1, 2, 5, and 6. The calculated results for power savings or loss, S , are listed in Table V and Table VII. The time ratio is equal to the peak load (3 s)

divided by the total time of operation, (12 s) and the duration of time for the sustained load (9 s) divided by the total time of operation. In the denominator of this equation, the maximum power between Model 1 and Model A is used.

Reduction of thermal mass by 17.5% (Model 3) results in power consumption decrease of 8.12%, reduction of thermal mass by 24% (Model 4) results in a power consumption decrease of 15.31%, removal of vacuum seal assumption (Model 5) results in a power consumption increase of 51.18% and use of stop-flow technique results in a power consumption decrease of 2.03%.

Obviously, power consumption due to radiation cannot be overlooked. However, radiation varies little with the design parameters studied here, namely, contact pad location and size, stop-flow technique and volume reduction. In fact, the only parameters that influence power loss due to radiation are vacuum sealing, which enhances radiation; and volume reduction, wherein external surface areas of the device are reduced, which result in reduced power consumption due to radiation. Specifically, radiation is invariant for Model 6 (0.20 W), since the dimensions of the preconcentrator device do not change for these models. On the other hand, small reductions in volume for Models 3 and 4 produce radiation values of 0.154 and 0.153 W, respectively, which are similar to those calculated for Model 1. If radiation is added to Model 1 values (vacuum seal included), peak and sustained power consumption is equal to 3.9 and 0.85 W, respectively, such that inclusion of radiation results in a power consumption increase of 18.9% in comparison with Model 1.

V. CONCLUSIONS AND FUTURE WORK

Clearly, reductions in thermal mass, and use of vacuum sealing produce the greatest power savings among design changes considered. The largest reductions in power consumption were obtained from vacuum sealing the device (51%) and reduction of thermal mass by removal of the outer silicon rings from the device (15.31%). We also found that varying contact pad size and/or location within the structure produced insignificant changes (<1%) in power consumption due to the relatively small size of the device. Implementation of the stop-flow technique provided only modest power savings (2.03%) to the device. Reduction in thermal mass, however, can only be accomplished with additional analyses, to assure both manufacturability and device structural stability.

The power consumed by the preconcentrator studied will be >1 W, whether or not radiative losses are considered. The total emissive power of a surface is dependent upon the material or substance, the surface condition (including roughness), and the temperature.⁴⁸ Reduction of radiation losses could be attained by use of a lower emissivity coating for the device or modification of surface roughness. Some workers, for example, have used surface texturing and anti-reflective thin films to reduce reflection of incident radiation for the purpose of enhancement of optical absorption.^{49,50} Others have shown that use of a reflective surface on the back of silicon crystal increases the apparent temperature,

when subjected to high heat fluxes.⁵¹ However, radiation is more efficient in a vacuum,³⁷ so use of a vacuum seal would unfortunately slightly increase radiative power losses.

We have demonstrated that scaling down the size of the preconcentrator device can lead to reduction in the overall energy [Wh] required for operation, but the number of electrochemistries required to satisfy large fluctuations in the power versus time curve can present more of a challenge in power selection than expected. We found several ongoing projects in the literature (e.g., biomaterial processing and detection,⁵² microgas separation columns⁹ and low-power consumption microheaters⁵³) which might benefit from this understanding.

Our concurrent efforts⁵⁴ have been in selecting hybrid power supplies, given the present limitations in reducing power spikes in this device. This work comprises selection of hybrid power supply strategy that accounts for both a high power density [W/L] power source for peaks/spikes in the power profile, and a high specific energy [Wh/kg] power source for long service.

ACKNOWLEDGMENTS

The authors would like to sincerely thank Professor R. D. Sacks for many enlightening discussions on gas chromatography, and both Professor S. Pang and Dr. W.-C. Tian for their input on design and fabrication of microdevices. This work was supported by the Engineering Research Centers Program of the National Science Foundation, Dr. Kensall Wise, PI.

¹C. J. Lu and E. T. Zellers, *Anal. Chem.* **73**, 3449 (2001).

²A. J. Grall, E. T. Zellers, and E. D. Sacks, *Environ. Sci. Technol.* **35**, 163 (2001).

³W. A. Groves, E. T. Zellers, and G. C. Frye, *Anal. Chim. Acta* **371**, 131 (1998).

⁴T. A. Ameal, I. Papautsky, R. O. Warrington, R. S. Wegeng, and M. K. Drost, *J. Propul. Power* **16**, 577 (2000).

⁵J. Whiting and R. Sacks, *Anal. Chem.* **74**, 246 (2002).

⁶A. J. Grall and R. D. Sacks, *Anal. Chem.* **71**, 5199 (1999).

⁷A. J. Grall and R. D. Sacks, *Anal. Chem.* **72**, 2507 (2000).

⁸C. Rossi, P. Temple-Boyer, and D. Esteve, *Sens. Actuators, A* **64**, 241 (1998).

⁹K. Robertson, *Sens. Actuators, A* **91**, 333 (2001).

¹⁰H. S. Noh, P. J. Hesketh, and G. C. Frye-Mason, *J. Microelectromech. Syst.* **11**, 718 (2002).

¹¹H. M. McNair and J. M. Miller, *Basic Gas Chromatography* (Wiley, New York, 1998).

¹²K. D. Wise and J. B. Angell, *NASA Technical Brief*, 1972.

¹³S. E. Terry, J. H. Jerman, and A. B. Angell, *IEEE Trans. Electron Devices* **ED-26**, 1880 (1979).

¹⁴I. Ciucanu and J. Pawliszyn, *Field Anal. Chem. Technol.* **5**, 69 (2001).

¹⁵Y. Kawamura, Y. Iwai, T. Yamanishi, S. Konishi, and M. Nishi, *Fusion Eng. Des.* **49**, 855 (2000).

¹⁶W. C. Tian and S. W. Pang, *J. Vac. Sci. Technol. B* **21**, 274 (2003).

¹⁷D. Vincenzi, M. A. Butturi, V. Guidi, M. C. Carotta, G. Martinelli, V. Guarnieri, S. Brida, B. Margesin, F. Giacomozzi, M. Zen, D. Giusti, G. Soncini, A. A. Vasiliev, and A. V. Pislakov, *J. Vac. Sci. Technol. B* **18**, 2441 (2000).

¹⁸D. D. Lee, W. Y. Chung, M. S. Choi, and J. M. Baek, *Sens. Actuators B* **33**, 147 (1996).

¹⁹Y. E. Wu, K. Chen, C. W. Chen, and K. H. Hsu, *Sens. Actuators, A* **100**, 37 (2002).

²⁰K. D. Wise, K. Najafi, and D. M. Aslam, *University of Michigan Project Proposal for National Science Foundation* (University of Michigan, Ann

- Arbor, 1999).
- ²¹S. Y. Wu, Q. Lin, Y. Yuen, and Y. C. Tai, *Sens. Actuators, A* **89** (2001).
- ²²U. Drechsler, N. Burer, M. Despont, U. Durig, B. Gotsmann, F. Robin, and P. Vettiger, *Microelectron. Eng.* **67–68** (2003).
- ²³D. J. Sadler, R. Changrani, P. Roberts, C. F. Chou, and F. Zenhausern, *IEEE Trans. Compon. Packag. Technol.* **26**, 309-316 (2003).
- ²⁴S. Mitra, Y. H. Xu, W. J. Chen, and A. Lai, *J. Chromatogr., A* **727**, 111 (1996).
- ²⁵J. M. Sanchez and R. D. Sacks, *Anal. Chem.* **75**, 978 (2003).
- ²⁶B. Zygmunt, *J. Chromatogr., A* **725**, 157 (1996).
- ²⁷I. Ciucanu, A. Caprita, A. Chiriac, and R. Barna, *Anal. Chem.* **75**, 736 (2003).
- ²⁸S. Mitra, N. H. Zhu, X. Zhang, and B. Kebbekus, *J. Chromatogr., A* **736**, 165 (1996).
- ²⁹S. Mitra, C. H. Feng, L. Zhang, W. Ho, and G. McAllister, *J. Mass Spectrom.* **34**, 478 (1999).
- ³⁰N. Zhu, Z. Li, and S. Mitra, *J. Microcolumn Sep.* **10**, 393 (1998).
- ³¹*Electric Resistance Heating* (British Electrical Development Association Inc., London, England, 1950).
- ³²D. D. Pollock, *Thermocouples: Theory and Properties* (CRC, Boca Raton, FL, 1991).
- ³³T. Veriotti and R. Sacks, *Anal. Chem.* **73**, 3045 (2001).
- ³⁴W. C. Tian, S. W. Pang, C. J. Lu, and E. Zellers, *J. Microelectromech. Syst.* **12**, 364 (2003).
- ³⁵Karlsson & Sorensen Hibbitt, Inc., (<http://www.abaqus.com>, USA, 2002).
- ³⁶J. N. Reddy, *Finite Element Method*, edited by J. J. Corrigan and J. M. Morriss, (McGraw-Hill, New York, 1993).
- ³⁷F. P. Incropera and D. P. DeWitt, *Fundamental of Heat and Mass Transfer*, 4th ed. (Wiley, New York, 1996).
- ³⁸N. M. Ravindra, B. Sopori, O. H. Gokce, S. X. Cheng, A. Shenoy, L. Jin, S. Abedrabbo, W. Chen, and Y. Zhang, *Int. J. Thermophys.* **22**, 1593-1611 (2001).
- ³⁹R. E. Meredith and C. W. Tobias, *Advances in Electrochemistry and Electrochemical Engineering*, edited by P. Delahay and C. W. Tobias, (Wiley, New York, 1961), p. 13.
- ⁴⁰M. Asheghi, K. Kurabayashi, R. Kasnavi, and K. E. Goodson, *J. Appl. Phys.* **91**, 5079 (2002).
- ⁴¹A. D. McConnell, S. Uma, and K. E. Goodson, *J. Microelectromech. Syst.* **10**, 360 (2001).
- ⁴²L. W. da Silva and M. Kaviani, "Micro Thermoelectric Cooler: Interfacial Effects on Thermal and Electrical Transport", *International Journal of Heat and Mass Transfer*, vol. 47(10-11), May 2004, pp. 2417-2435.
- ⁴³J. C. Thompson and A. Younglove, *J. Phys. C* **20**, 112 (1961).
- ⁴⁴R. D. Sacks (unpublished).
- ⁴⁵D. R. Sparks, S. Massoud-Ansari, and N. Najafi, *IEEE Trans. Adv. Packag.* **26**, 277 (2003).
- ⁴⁶B. Lee, S. Seok, and K. Chun, *J. Micromech. Microeng.* **13**, 663 (2003).
- ⁴⁷R. Gooch, T. Schimert, W. McCardel, B. Ritchey, D. Gilmour, and W. Koziarz, *J. Vac. Sci. Technol. A* **17**, 2295 (1999).
- ⁴⁸D. R. Pitts and L. E. Sisson, *Schaum's Outline of Theory and Problems of Heat transfer*, 2nd Ed. (McGraw-Hill, New York, 1998).
- ⁴⁹E. S. Kolesar, V. M. Bright, and D. M. Sowders, *Thin Solid Films* **270**, 10-15 (1993).
- ⁵⁰D. Minkov, *Sol. Energy Mater. Sol. Cells* **31**, 323-335 (1993).
- ⁵¹R. K. Smither and P. B. Fernandez, *Nucl. Instrum. Methods Phys. Res. A* **347**, 313-319 (1994).
- ⁵²H. J. H. Chen, T. F. Chen, S. R. S. Huag, J. Gong, J. C. Li, W. C. Chen, and T. H. Hseu, and I. C. Hsu, *Sens. Actuators, A* **108**, 193-200 (2003).
- ⁵³G. S. Chung, *Sens. Actuators, A* **112**, 55-60 (2004).
- ⁵⁴K. A. Cook and A. M. Sastry, *J. Power Sources* **140**, 181-202 (2005).